Modulation of Western North Pacific Tropical Cyclone Activity by the Atlantic Meridional Mode

W. Zhang [1,2,*], G. A. Vecchi[1,2], G. Villarini[3], H. Murakami[1,2],
A. Rosati[1], X. Yang[1,4], L. Jia[1,2], and F. Zeng[1]

[1]National Oceanic and Atmospheric Administration/Geophysical Fluid Dynamics Laboratory, Princeton, NJ, USA
[2]Atmospheric and Oceanic Sciences Program, Princeton University, Princeton, NJ, USA
[3] IIHR-Hydroscience & Engineering, The University of Iowa, Iowa City, Iowa
[4]University Corporation for Atmospheric Research, Boulder, Colorado

To be submitted to Climate Dynamics

*Corresponding author:
Wei Zhang, Ph.D.
National Oceanic and Atmospheric Administration/Geophysical Fluid Dynamics Laboratory and Atmospheric and Oceanic Sciences Program, Princeton University, Princeton, NJ, USA, 08540
Phone: 609-452-5817
Email: wei.zhang@noaa.gov

Abstract

This study examines the year-to-year modulation of the western North Pacific (WNP) tropical cyclones (TC) activity by the Atlantic Meridional Mode (AMM) using both observations and the Geophysical Fluid Dynamics Laboratory (GFDL) Forecast-oriented Low Ocean Resolution Version of CM2.5 (FLOR) global coupled model. 1. The positive (negative) AMM phase suppresses (enhances) WNP TC activity in observations. The anomalous occurrence of WNP TCs results mainly from changes in TC genesis in the southeastern part of the WNP. 2. The observed responses of WNP TC activity to the AMM are connected to the anomalous zonal vertical wind shear (ZVWS) caused by AMM-induced changes to the Walker circulation. During the positive AMM phase, the warming in the North Atlantic induces strong descending flow in the tropical eastern and central Pacific, which intensifies the Walker cell in the WNP. The intensified Walker cell is responsible for the suppressed (enhanced) TC genesis in the eastern (western) part of the WNP by strengthening (weakening) ZVWS. 3. The observed WNPTC-AMM linkage is examined by the long-term control and idealized perturbations experiment with FLOR-FA. A suite of sensitivity experiments strongly corroborate the observed WNPTC-AMM linkage and underlying physical mechanisms.

1. Introduction

Tropical cyclones (TCs) are among the most destructive and costly natural disasters (e.g., Rappaport, 2000; Pielke Jr et al., 2008; Zhang et al., 2009). Understanding and predicting the status of TC occurrence is a topic of intense scientific interest (e.g., Mitchell, 1932; Gray, 1979; Vitart and Stockdale, 2001; Klotzback, 2007; Vecchi et al., 2014).

Environmental factors affecting the status of TC genesis in the western North Pacific (WNP) are strongly modulated by the sea surface temperature (SST) modes such as the El Niño Southern Oscillation (ENSO) (e.g., Chan, 1985; Wu and Lau, 1992; Chan, 2000; Wang and Chan, 2002; Camargo and Sobel, 2005; Zhang et al., 2012; 2015a; 2015c), the North Pacific Gyre Oscillation (Zhang et al., 2013), the Pacific Meridional Mode (Zhang et al., 2015b), the Pacific Decadal Oscillation (PDO; Lee et al., 2012; Liu and Chan, 2012; Girishkumar et al., 2014) and basin-wide Indian ocean SST changes (Du et al., 2010; Zhan et al., 2010; Zhan et al., 2014). Therefore, the SST patterns in both Pacific and other ocean basins can alter the occurrence of WNP TCs through both local forcing and remote teleconnections. A number of studies have documented the importance of the North Atlantic SST in mediating Pacific climate including the Walker circulation (England et al., 2014; McGregor et al., 2014), ENSO (Ham et al., 2013; Yu et al., 2014), and the PDO (Zhang and Delworth, 2007; Zhang and Zhu, 2015). The SST anomalies in the North Atlantic have been recently found to exhibit substantial statistical connection with WNP TC activity (Li et al., 2013; Huo et al., 2015; Yu et al., 2015). More specifically, positive

SST anomalies in the North Atlantic tend to suppress TC activity in the WNP (Li et al., 2013; Huo et al., 2015; Yu et al., 2015). Yu et al. (2015) proposed the Indian Ocean relay effect for interpreting the link between North Atlantic SST anomalies and WNP TCs. Huo et al. (2015) analyzed observed statistical relationships between Atlantic SST and the key dynamic and thermodynamic conditions in the WNP to interpret the impacts of North Atlantic SST on WNP TCs; yet the underlying physical mechanisms connecting the Atlantic to these large-scale WNP changes were not provided in their study. Therefore, while there is mounting evidence supporting the idea that North Atlantic SST influences the occurrence of WNP TCs, the field is still attempting to disentangle the underlying physical mechanisms.

The Atlantic Meridional Mode (AMM) is a leading mode of the coupled ocean/atmosphere system in the tropical & subtropical Atlantic (Nobre and Shukla, 1996; Chang et al., 1997; Chiang and Vimont, 2004; Vimont and Kossin, 2007; Smirnov and Vimont, 2010). The AMM has also been referred to historically as the Atlantic Dipole or Inter-hemispheric Mode (Servain, 1991; Xie and Philander, 1994; Carton et al., 1996) or the tropical Atlantic gradient mode (Chiang et al., 2002). The AMM exhibits variability on a variety of time scales from inter-annual to decadal. On decadal scales, the AMM is closely linked to the Atlantic Multidecadal Oscillation (AMO) (Kossin and Vimont, 2007; Vimont and Kossin, 2007; Grossmann and Klotzbach, 2009). While it has been shown that the AMM modulates hurricane activity in the North Atlantic (Vimont and Kossin, 2007), here we examine whether, the extent to which and by what mechanisms changes in the phase and magnitude of

AMM can modulate WNP TC activity. By using the long-term control experiments of the Geophysical Fluid Dynamics Laboratory (GFDL) Forecast-oriented Low Ocean Resolution Version of CM2.5 (FLOR), we can test the robustness of the observed linkage between WNP TC activity and AMM and explore the mechanisms behind the connection. This study will advance our understanding of TC activity in the WNP, and provide references for the prediction and projection of WNP TC activity.

The remainder of this paper is organized as follows. Section 2 presents methodology and Section 3 discusses the analysis results based on observation and simulation results. Section 4 includes the discussion and conclusion.

2. Data and Methodology

2.1 Data

The TC data are obtained from International Best Track Archive for Climate Stewardship (IBTrACS; Knapp et al., 2010). We focus on WNP TCs that occur in the peak season (June to November: JJASON). The key meteorological variables such as zonal and meridional wind fields, geopotential height, vorticity and relative humidity are from the Japan Meteorology Agency (JMA) 55 reanalysis data (JRA-55, Kobayashi et al., 2015). To substantiate the results, the National Centers for Environmental Prediction and the National Center for Atmospheric Research (NCEP/NCAR; Kalnay et al., 1996) reanalysis data are also used. The JRA-55 is available since 1958 on a global basis with a spatial resolution of 1.25° × 1.25°. It is based on a new data assimilation system that reduces many of the problems reported in the first JMA reanalysis (Kobayashi et al., 2015). The zonal vertical wind shear

(|du/dz| or $|u_z|$) is defined as the magnitude of the differences in zonal wind between 200 hPa and 850 hPa level. Monthly estimates of SST are taken from the Met Office Hadley Centre HadSST3.1.1.0 (Kennedy et al., 2011).

2.2 AMM Index

The AMM index is calculated following Chiang and Vimont (2004) by the singular value decomposition (SVD) of 10m surface wind fields (zonal and meridional components) and SST. In its calculation, the seasonal cycle and the linear trend are first removed by applying a three-month running mean to the data, and then subtracting the linear fit to the cold tongue index (CTI, Deser and Wallace, 1987) from every single spatial point to remove correlations with El Niño (Chiang and Vimont, 2004). The CTI is defined as the average SST anomaly over 6°N - 6°S, 180 - 90°W (Deser and Wallace, 1987). The regression of SST and 10m surface wind fields onto the AMM index (i.e., the PC time series) represents the spatial patterns during the positive AMM phase (Figure 1). The warming and cooling patterns of SST stride the equator and are coupled with surface winds (Figure 1). To further validate the independence of AMM on ENSO, we also show the AMM pattern during neutral ENSO years (Figure 1b). The El Niño (La Niña) years are defined as those with the Niño 3 values during June-November larger (smaller) than 1 (-1) standard deviation.

2.3 Global Coupled Model

This study employs a newly-developed high-resolution coupled climate model for experiments, the Geophysical Fluid Dynamics Laboratory (GFDL) Forecast-oriented Low Ocean Resolution Version of CM2.5 (FLOR) (e.g., Vecchi et al., 2014; Jia et al., 2015; Yang et al., 2015). This model is characterized by high-resolution land and atmosphere components but relatively low-resolution ocean component (Vecchi et al., 2014). The atmosphere and land are the same as those of the GFDL Climate Model version (CM) 2.5 (CM2.5; Delworth et al., 2012) with a spatial resolution of 50 km × 50 km. The ocean and sea ice components of FLOR are similar to those in the CM2.1 (Delworth et al., 2006) with a spatial resolution of 1×1 degree. The relatively low spatial resolution of the ocean and sea ice components in FLOR enables large ensembles and better efficiency for seasonal forecasting. This study utilizes the flux-adjusted version of FLOR (FLOR-FA) for sensitivity experiments in which climatological adjustments are applied to the model's momentum, enthalpy and freshwater flux from the atmosphere to the ocean to give the model's SST and surface wind stress a closer climatology to the observations over 1979-2012 (Vecchi et al., 2014). For more details about the FLOR model, please refer to Vecchi et al. (2014), Jia et al. (2015), Yang et al. (2015) and references therein.

2.4 Control simulation

A 3500-year long control simulation was performed with the FLOR-FA by prescribing radiative forcing representative of 1860. These experiments are referred to as "Pre-industrial" experiments with FLOR-FA. Here we focus on the first 1000 years for the analysis of AMM and TCs for the sake of computing efficiency. We compared the results based on the first 1000 years from those derived from the other 2500 years and the results are consistent. The 500-year control simulation by prescribing radiative forcing and land use representative of 1990 with FLOR-FA is also analyzed to characterize the AMM-TC association. Because the AMM-TC association based on FLOR-FA 1990 is consistent with that on FLOR-FA 1860, this study only shows results based on FLOR-FA 1860.

2.5 Perturbation Experiments

A reference climatological experiment (CLIMO) is prepared by nudging the SSTs in FLOR to the repeating annual cycle of global climatological SST from the long-term control experiment of FLOR-FA; the perturbation experiment (PAMM) is designed by prescribing the annual cycle of climatological SST outside the AMM region and the overlapping of the annual cycle of climatological SST and SST anomalies associated with the positive AMM mode inside the AMM region. SST in both experiments is restored to each target with 5-day time scale. The subtraction of the control experiment from the perturbation experiment (PAMM minus CLIMO) produces the net influence of the positive AMM mode. Because GFDL FLOR is a TC-resolving model, we use a tracker to extract TCs from the simulated output. Both CLIMO and PAMM experiments spin up for 100 years and further integrated for 60 years.

2.6 Tracking algorithm

TCs in FLOR are tracked from 6-hourly model output by using the tracker developed at GFDL and this tracker has been implemented in Murakami et al. (2015) and Zhang et al. (2015b,c). The temperature anomaly averaged vertically over 300 and 500 hPa (t_a), 10 m wind speed, 850 hPa relative vorticity and sea level pressure (SLP) are key factors of this tracker. The tracking procedures are as follows.

(1) Find local minima of the smoothed SLP field. The location of the cyclone center is properly adjusted by fitting a biquadratic surface to the SLP and locating the center at the minima.

(2) Closed contours are in an interval of 2 hPa (dp) around every single low center. The N^{th} contour is marked as the contiguous region surrounding a low central pressure P with pressures lower than dp × N + P, as detected by a "flood fill" algorithm. Note that the contours are not required to be circular and a maximum radius of 3,000 km is searched from each candidate SLP low center.

(3) If the above closed contours are found, the low is counted as a TC center. In this way, the tracker attempts to find all closed contours within a certain distance of the low center and without entering contours belonging to another low. The maximum 10-m wind inside the set of closed contours is taken as the maximum wind speed at that time for the storm.

(4) Warm cores are detected via similar processes: closed 1K contours are found surrounding the maximum t_a within a TC's identified contours, no more than 1 degree from the low center. This contour must have a radius smaller than 3 degrees in distance. If such a core is not found, it is not considered as a warm-core low center and the center is rejected.

(5) TC centers are combined into a TC track by taking a low center at time T - dt, extrapolating its motion forward dt, and then seeking for storms within 750 km. A deeper low center has higher priority of tracking.

(6) The following criteria are required to finalize the TC identifications.

a. At least 72 hours of total detection lifetime (not necessarily consecutive).
b. At least 48 cumulative (not necessarily consecutive) hours with a warm core.
c. At least 36 consecutive hours of a warm core with winds greater than 17.5 ms^{-1}.
d. TC genesis should be confined equatorward of 40°N.

TC track/genesis density in the WNP is binned into 5° × 5° grid boxes at a 6-hour interval without smoothing.

3. Analysis Results

3.1 Results from Observations

We start with the analysis of AMM which is derived from observed SST data. The full AMM index exhibits an increasing trend over 1970-2013, but we explore the detrended time series to focus on the year-to-year variations (Figure 2a). The detrended AMM index has a significant correlation (-0.41) with WNP TC frequency for 1970-2013 at 0.01 level of significance, reflecting a tendency for WNP TC frequency to be suppressed (enhanced) in the positive (negative) AMM phase (Figure 2a). We do not consider autocorrelation in the calculation of the correlation between the WNP TC frequency and the AMM index because the autocorrelations for WNP TC frequency and the AMM index are statistically insignificant. The slope of the linear least square fit line for all years (1970-2013) is almost the same as the one for only the neutral ENSO years during this period, indicating that ENSO does not strongly influnence the WNPTC-AMM association (Figure 2b).

More details of the relationship of the AMM with WNP TC can be seen in the regression of TC track density onto the detrended AMM index for the period 1970-2013, which shows negative loading in almost the entire WNP (Figure 3a). In addition, the regression of TC genesis density onto AMM features negative anomalies in the WNP except the regions from 130°E to 145°E in the southwestern WNP (Figure 3b). Moreover, the regression of basinwide TC genesis anomalies onto AMM is negative. The spatial regression of both WNP TC density and genesis onto the AMM index, along with the correlation of basinwide frequency with AMM, indicates a significant link between AMM and WNP TC activity. The southeastern part of the WNP has long been considered a key region for WNP TC genesis (Chan, 2000; Wang and Chan, 2002; Camargo et al., 2007).

Previous studies have highlighted the dominant role of zonal vertical wind shear (ZVWS) induced by remote SST, instead of local SST, in modulating WNP TC genesis (Wang and Chan, 2002; Chan and Liu, 2004). The regression of TC genesis density onto AMM shows similarities with that of the genesis potential index (GPI) (Emanuel and Nolan, 2004; Camargo et al., 2007) (Figures 3b and 4a). Specifically, the regression of GPI onto the AMM index is characterized by negative anomalies in the eastern WNP and positive anomalies in the western WNP (Figure 4a). Among the factors associated with GPI, ZVWS stands out to agree with the spatial patterns of GPI while 600-hPa relative humidity and 850-hPa relative vorticity are not consistent with the spatial patterns of GPI (Figure 4b,d). To further assess the underlying mechanisms, we analyze the Walker circulation, represented by the vertical profile of vertical pressure velocity and zonal wind averaged over 0-20 °N where most of WNP TCs are formed. The anomalous ZVWS is associated with an anomalous regional Walker cell in the WNP (120°E-180°E) (Figure 4e). An anomalously ascending (reduced subsidence) branch in the western WNP (120°E-150°E) is accompanied with an anomalously descending (reduced ascent) branch in the eastern WNP (150°E-180°E) (Figure 4e). This anomalous zonal circulation would intensify ZVWS, and act to suppress TC activity in the eastern WNP during the positive AMM phase because the climatology of lower level and upper level winds are largely easterly and westerly respectively in the western part of the WNP (Figure 4e).

There are enhanced TC geneses in the western WNP during positive AMM phases (Figure 3b). Such TC geneses are associated with weakened ZVWS in this region. The weakened ZVWS is caused by the displaced Walker circulation because the climatology of lower and upper level winds are largely westerly and easterly respectively in the western WNP (Figure 4e). The altered Walker circulation tends to weaken the prevalent upper easterly and it also weakens the lower westerly to some degree, resulting in weakened ZVWS in the western WNP (Figure 4d,e). A number of studies have found that Atlantic SST anomalies could act to modulate the Pacific Walker circulation and trades in the tropical Pacific by displacing the Walker circulation (Kucharski et al., 2011; Ham et al., 2013; McGregor et al., 2014), providing a plausible mechanism for the relationships observed in this section.

3.2 Control experiments

To investigate the mechanisms connecting the AMM and WNP TCs, we first assess whether the TC-AMM association holds in the long-term control experiment in a coupled climate model (FLOR-FA 1860). The fundamental structures of the observed AMM mode (i.e., a dipole mode of SST coupled with surface winds) are captured in the long-term control experiment of FLOR-FA (Figure 5) as they were in a related model (GFDL CM2.5) (Doi et al., 2013). Previous studies have found that the positive and negative SST anomalies related to AMM are not strongly connected to one another (e.g., Chiang and Vimont, 2004). This is also consistent with the interpretation of meridional mode as an extratropics-to-tropics linkage (Chiang and Vimont, 2004; Zhang et al., 2014).

Figure 6 depicts the histogram of the correlation coefficients between WNP TC frequency and the AMM index in every 45-year chunk of the 1000-year control simulation. The mean of the correlation coefficients is around -0.21 which is statistically different from 0 at 0.01 level of significance based on the Student's t-test. (Figure 6), although the simulated WNPTC-AMM association is weaker than the observed one (the red vertical line in Figure 6).

For further analysis, we classify the 1000 years into the positive and negative AMM years with the magnitude of AMM index averaged over JJASON larger than one standard deviation. There are significantly fewer WNP TCs during the positive AMM years compared to the negative AMM years (Figure 7). The anomalies of WNP TC frequency are defined as the deviation from the average WNP TC frequency over the 1000 years. The TC frequency difference in the southeastern portion of the WNP is mainly responsible for the difference in total WNP TC frequency between two

AMM phases (Figure 7), consistent with the observed spatial pattern of TC genesis (Figure 3). The regression of TC track density onto the AMM index is characterized by negative anomalies in the WNP; on the other hand, the regression of TC genesis density in the long-term control experiment has characteristic negative anomalies only in the southeastern portion of the WNP with weak positive anomalies in its southwestern portion (Figure 8). The positive anomalies in TC genesis in the southwestern part of WNP in the control experiment is weaker than those in the observations (Figures 3 and 8).

To disentangle the physical mechanisms underlying how AMM modulates WNP TC activity in the control experiment, we also regress the genesis potential index (GPI), 600-hPa relative humidity, 850-hPa relative vorticity, ZVWS and vertical atmospheric velocity onto AMM during strong AMM years as what is shown for observations. The regression of the GPI pattern onto AMM is consistent with the pattern of TC genesis (Figures 8b and 9a). Among the key atmospheric variables relevant to GPI, ZVWS stands out to be linked with GPI because of the similarity in the regression of ZVWS and GPI onto AMM (Figure 9). Previous studies have highlighted the key role of ZVWS in modulating TC genesis in the WNP (Wang and Chan, 2002; Chan and Liu, 2004), supporting our results both in the observations and long-term control experiment of FLOR-FA .

We find that ZVWS is changed mostly by the displacement of the Walker circulation in the WNP in the observations. Figure 9e shows that an anomalous Walker cell resides from the eastern part of the WNP to the eastern Pacific (140°E to

100°W). To the east of this Walker cell, there is another anomalous Walker cell with descending branch located around 100°W, which is associated with the warming during positive AMM phase (Figure 9e). We speculate that the AMM induces a displacement of the Walker circulation, which is responsible for changes in ZVWS in the WNP including strengthened ZVWS in the eastern WNP and weakened ZVWS in the western WNP (Figure 9e). The climatology of zonal wind in control experiment is similar to that in observations (Figures 4e and 9e). The altered Walker circulation is responsible for the intensified ZVWS in the eastern WNP by strengthening the prevalent (climatological) upper level westerly and lower level easterly and for the diminished ZVWS in the western WNP by weakening the prevalent (climatological) upper level easterly and lower level westerly (Figures 9e). The anomalous ZVWS subsequently modulates WNP TC genesis. Such mechanisms are consistent with those based on observations. A suite of experiments using the state-of-the-art GFDL FLOR-FA coupled climate model are performed to verify the mechanisms underlying how AMM regulates WNP TC genesis.

3.3 Sensitivity experiments

To verify the mechanisms underlying how the AMM influences TC activity in the WNP, we have performed a suite of experiments including the control experiment and the perturbation experiment using FLOR-FA (Jia et al., 2015; Vecchi et al., 2014; Yang et al., 2015). The control and perturbation experiments are denoted as CLIMO and PAMM, respectively. The details of both experiments are provided in Section 2.

The PAMM experiment produces significantly fewer (3.7 times) WNP TCs than the CLIMO experiment (Table 1). It appears that the suppressed WNP TC genesis in the PAMM experiment is due to suppressed TC activity in the southeastern part of the WNP (Table 1). In addition, TC genesis in the northeastern part is also suppressed in the PAMM phases, even though the PAMM experiment produces more TC geneses in the southwestern part of the WNP (Table 1). Such forced TC responses are further supported by the differences in the spatial pattern of TC track and genesis density between PAMM and CLIMO experiments (Figure 10).

The forced anomalous TC density responses to PAMM strongly resemble that in the long-term control experiment (Figure 10a), though there are some weak positive TC density anomalies from the Philippines to Vietnam in the PAMM experiment. The subtraction of TC genesis density in the PAMM from CLIMO experiment produces anomalous negative anomalies in the eastern WNP and positive anomalies in a large portion of the western WNP, consistent with the observed TC genesis density anomalies in the observations (Figures 3b and 10b). The negative TC genesis density anomalies in PAMM are located slightly eastward compared to the observations and this may be caused by the biases in simulated TC track density with FLOR or CM2.5 (Kim et al., 2014; Vecchi et al., 2014). The differences in the spatial pattern of TC genesis between PAMM and CLIMO experiments (Figure 10) are consistent with what shown in Table 1. The PAMM experiment has less TC geneses in the southeastern portion and more TC geneses in the southwestern portion of the WNP than the CLIMO experiment (Figure 10b), consistent with the results based on observations and the long-term control run with FLOR-FA.

To assess the role of key large-scale environmental variables in WNP TC genesis, we have analyzed the differences in GPI, relative humidity, 850 hPa relative vorticity, ZVWS and the Walker circulation between PAMM and CLIMO experiments (Figure 11). The sensitivity experiments reproduce the relationship between key variables and GPI in observations and long-term control experiment (Figures 4, 9 and 11). Negative GPI anomalies are located in the southeastern WNP while positive GPI anomalies are located in the southwestern WNP (Figure 11a). The ZVWS differences between PAMM and CLIMO are characterized by positive anomalies in the southeastern WNP and negative anomalies in the southwestern WNP (Figure 11d), consistent with the spatial patterns of GPI (Figure 11a). The anomalous Walker circulation in the PAMM experiment shows similarity with what shown in the observations: there is an anomalous ascending branch in the Atlantic and a descending branch in the central Pacific forced by warming during the positive AMM phases, which act to enhance the ascending branch in the eastern WNP (Figure 11e). Such displacement of the Walker circulation leads to the anomalous Walker cell residing from the western to tropical central Pacific; this is responsible for the enhanced ZVWS in the eastern part of WNP and the diminished ZVWS in the western part of the WNP during the positive AMM phase (Figure 11e). The anomalous Walker circulation in PAMM is located in a slightly different location compared to the observations. For example, the descending branch of the Walker circulation in the western WNP resides slightly westward compared with observations (Figures 4e and 10e).

The two experiments (CLIMO and PAMM) therefore strongly support the physical mechanisms underlying the observed AMM-TC association. During the positive AMM phases, the anomalous SST warming in the North Atlantic forces changes in the atmospheric Walker circulation, which intensifies ZVWS in the eastern part of the WNP and suppresses TC genesis there.

4. Discussion and conclusion

Several studies have highlighted the important role of the North Atlantic SST in modulating WNP TC activity (e.g., Huo et al., 2015; Yu et al., 2015). The forcing impacts of remote tropical SST on TC activity have been identified in the North Atlantic and WNP (Vecchi and Soden, 2007; Lin and Chan, 2015). This study further examines the possible year-to-year modulation of WNP TC activity by AMM. Our research findings are summarized as follows.

1. The positive (negative) AMM phase suppresses (enhances) WNP TC activity in the observations. The anomalous occurrence of WNP TCs results mainly from changes in TC genesis in the southeastern part of the WNP.

2. The observed responses of WNP TC activity to the AMM phase are connected to the anomalous ZVWS driven by AMM-induced changes to the Walker circulation. During the positive AMM phase, the warming in the North Atlantic induces strong descending flow in the tropical eastern and central Pacific, which intensifies the Walker cell in the eastern WNP. The intensified Walker cell is responsible for the suppressed TC genesis in the eastern part of the WNP by strengthening ZVWS.

3. The observed WNPTC-AMM linkage is supported by the long-term control and idealized perturbations experiment with FLOR-FA. A suite of sensitivity experiments strongly corroborate the observed WNPTC-AMM linkage and underlying physical mechanisms.

The WNPTC-AMM linkage will provide useful references for the prediction of WNP TC frequency by combining with other factors such as PMM, Niño 4 and the South Oscillation Index (Chan et al., 2001; Fan and Wang, 2009). This study has identified the important role of AMM in mediating WNP TC activity, confirming the impacts of the Atlantic SST on WNP TCs (Huo et al., 2015; Yu et al., 2015). AMM influences WNP TC activity via changing ZVWS in the WNP (especially in the southeastern and southwestern portions) by altering the Walker circulation. Therefore, this study has also proposed new physical mechanisms to interpret the linkage between AMM and WNP TC activity. Such underlying mechanisms are supported by observations, long-term control experiments and a suite of sensitivity experiments with the state-of-the-art FLOR-FA coupled climate model.

TC Frequency in the WNP has sharply decreased since the late 1990s (Tu et al., 2009; Liu and Chan, 2012; Choi et al., 2015; He et al., 2015; Lin and Chan, 2015). Such changes have been attributed to suppressed TC genesis in the southeastern part of the WNP (Liu and Chan, 2012; He et al., 2015; Lin and Chan, 2015; Wu et al., 2015). The Atlantic SST has been warming since 1950s and the multi-decadal change of the Atlantic SST (e.g., AMO) plays an important role in the rising SST. Based on our research findings, the suppressed TC activity in the WNP may be caused by the rising SST in the North Atlantic since the mid-1990s. This will be examined in our future work. PMM also exerts strong impacts on WNP TC activity (Zhang et al., 2015b). PMM enhances TC genesis in the WNP, especially in the southeastern WNP by inducing the Matsuno-Gill responses to the heating relevant to the northwestern part of the positive PMM pattern. Our ongoing research is examining how concurrent AMM and PMM influence WNP TC activity.

Despite the advancements made in understanding WNP TC activity, there are several caveats to be addressed. First, this study is limited by the uncertainties and biases in the simulations of FLOR-FA. Second, due to the inherent complexity existing in WNP TC activity, AMM is just one factor/mode that modulates WNP TCs. The concurrent influences of AMM, PMM, ENSO and even East Indian Ocean SST on WNP TCs should be considered to obtain a more comprehensive understanding.

Acknowledgement

The authors thank Lakshmi Krishnamurthy and Honghai Zhang for their comments that improve an earlier version of this manuscript. This material is based in part upon work supported by the National Science Foundation under Grants AGS-1262091 and AGS-1262099.

References

Camargo, S. J. and A. H. Sobel, 2005: Western North Pacific tropical cyclone intensity and ENSO. Journal of Climate, 18, 2996-3006.

Camargo, S. J., K. A. Emanuel, and A. H. Sobel, 2007: Use of a Genesis Potential Index to Diagnose ENSO Effects on Tropical Cyclone Genesis. Journal of Climate, 20, 4819-4834.

Camargo, S. J., A. H. Sobel, A. G. Barnston, and K. A. Emanuel, 2007: Tropical cyclone genesis potential index in climate models. Tellus A, 59, 428-443.

Carton, J. A., X. Cao, B. S. Giese, and A. M. Da Silva, 1996: Decadal and Interannual SST Variability in the Tropical Atlantic Ocean. Journal of Physical Oceanography, 26, 1165-1175.

Chan, J. C. L., J. Shi, and K. S. Liu, 2001: Improvements in the Seasonal Forecasting of Tropical Cyclone Activity over the Western North Pacific. Weather and Forecasting, 16, 491-498.

Chan, J. C. L., 1985: Tropical Cyclone Activity in the Northwest Pacific in Relation to the El Nino Southern Oscillation Phenomenon. Monthly Weather Review, 113, 599-606.

Chan, J. C. L., 2000: Tropical cyclone activity over the western North Pacific associated with El Nino and La Nina events. Journal of Climate, 13, 2960-2972.

Chan, J. C. L. and K. S. Liu, 2004: Global Warming and Western North Pacific Typhoon Activity from an Observational Perspective. Journal of Climate, 17, 4590-4602.

Chang, P., L. Ji, and H. Li, 1997: A decadal climate variation in the tropical Atlantic Ocean from thermodynamic air-sea interactions. Nature, 385, 516-518.

Chiang, J. C. H. and D. J. Vimont, 2004: Analogous Pacific and Atlantic Meridional Modes of Tropical Atmosphere–Ocean Variability*. Journal of Climate, 17, 4143-4158.

Chiang, J. C. H., Y. Kushnir, and A. Giannini, 2002: Deconstructing Atlantic Intertropical Convergence Zone variability: Influence of the local cross-equatorial sea surface temperature gradient and remote forcing from the eastern equatorial Pacific. Journal of Geophysical Research: Atmospheres, 107, ACL 3-1-ACL 3-19.

Choi, Y., K.-J. Ha, C.-H. Ho, and C. Chung, 2015: Interdecadal change in typhoon genesis condition over the western North Pacific. Climate Dynamics, 1-13.

Delworth, T. L., A. Rosati, W. Anderson, A. J. Adcroft, V. Balaji, R. Benson, K. Dixon, S. M. Griffies, H.-C. Lee, R. C. Pacanowski, G. A. Vecchi, A. T. Wittenberg, F. Zeng, and R. Zhang, 2012: Simulated Climate and Climate Change in the GFDL CM2.5 High-Resolution Coupled Climate Model. Journal of Climate, 25, 2755-2781.

Delworth, T. L., A. J. Broccoli, A. Rosati, R. J. Stouffer, V. Balaji, J. A. Beesley, W. F. Cooke, K. W. Dixon, J. Dunne, K. A. Dunne, J. W. Durachta, K. L. Findell, P. Ginoux, A. Gnanadesikan, C. T. Gordon, S. M. Griffies, R. Gudgel, M. J. Harrison, I. M. Held, R. S. Hemler, L. W. Horowitz, S. A. Klein, T. R. Knutson, P. J. Kushner, A. R. Langenhorst, H.-C. Lee, S.-J. Lin, J. Lu, S. L. Malyshev, P. C. D. Milly, V. Ramaswamy, J. Russell, M. D. Schwarzkopf, E. Shevliakova, J. J. Sirutis, M. J. Spelman, W. F. Stern, M. Winton, A. T. Wittenberg, B. Wyman, F. Zeng, and R. Zhang, 2006: GFDL's CM2 Global Coupled Climate Models. Part I: Formulation and Simulation Characteristics. Journal of Climate, 19, 643-674.

Deser, C. and J. M. Wallace, 1987: El Niño events and their relation to the Southern Oscillation: 1925–1986. Journal of Geophysical Research: Oceans, 92, 14189-14196.

Doi, T., G. A. Vecchi, A. J. Rosati, and T. L. Delworth, 2013: Response to CO2 Doubling of the Atlantic Hurricane Main Development Region in a High-Resolution Climate Model. Journal of Climate, 26, 4322-4334.

Du, Y., L. Yang, and S.-P. Xie, 2010: Tropical Indian Ocean Influence on Northwest Pacific Tropical Cyclones in Summer following Strong El Niño*. Journal of Climate, 24, 315-322.

Emanuel, K. A. and D. Nolan, 2004: Tropical cyclone activity and the global climate system. Preprints, 26th Conf. on Hurricanes and Tropical Meteorology, Miami, FL, Amer. Meteor. Soc. A.

England, M. H., S. McGregor, P. Spence, G. A. Meehl, A. Timmermann, W. Cai, A. S. Gupta, M. J. McPhaden, A. Purich, and A. Santoso, 2014: Recent intensification of wind-driven circulation in the Pacific and the ongoing warming hiatus. Nature Clim. Change, 4, 222-227.

Fan, K. and H. Wang, 2009: A New Approach to Forecasting Typhoon Frequency over the Western North Pacific. Weather and Forecasting, 24, 974-986.

Girishkumar, M. S., V. P. Thanga Prakash, and M. Ravichandran, 2014: Influence of Pacific Decadal Oscillation on the relationship between ENSO and tropical cyclone activity in the Bay of Bengal during October–December. Climate Dynamics, 1-11.

Gray, W. M., 1979: Hurricanes: Their formation, structure and likely role in the tropical circulation. Meteorology over the tropical oceans, 77, 155-218.

Grossmann, I. and P. J. Klotzbach, 2009: A review of North Atlantic modes of natural variability and their driving mechanisms. Journal of Geophysical Research: Atmospheres, 114, n/a-n/a.

Ham, Y.-G., J.-S. Kug, J.-Y. Park, and F.-F. Jin, 2013: Sea surface temperature in the north tropical Atlantic as a trigger for El Nino/Southern Oscillation events. Nature Geoscience, 6, 112-116.

He, H., J. Yang, D. Gong, R. Mao, Y. Wang, and M. Gao, 2015: Decadal changes in tropical cyclone activity over the western North Pacific in the late 1990s. Climate Dynamics, 1-13.

Huo, L., P. Guo, S. N. Hameed, and D. Jin, 2015: The role of tropical Atlantic SST anomalies in modulating western North Pacific tropical cyclone genesis. Geophysical Research Letters, 2015GL063184.

Jia, L., X. Yang, G. A. Vecchi, R. G. Gudgel, T. L. Delworth, A. Rosati, W. F. Stern, A. T. Wittenberg, L. Krishnamurthy, S. Zhang, R. Msadek, S. Kapnick, S. Underwood, F. Zeng, W. G. Anderson, V. Balaji, and K. Dixon, 2015: Improved Seasonal Prediction of Temperature and Precipitation over Land in a High-Resolution GFDL Climate Model. Journal of Climate, 28, 2044-2062.

Kalnay, E., M. Kanamitsu, R. Kistler, W. Collins, D. Deaven, L. Gandin, M. Iredell, S. Saha, G. White, and J. Woollen, 1996: The NCEP/NCAR 40-year reanalysis project. Bulletin of the American Meteorological Society, 77, 437-471.

Kennedy, J. J., N. A. Rayner, R. O. Smith, D. E. Parker, and M. Saunby, 2011: Reassessing biases and other uncertainties in sea surface temperature observations measured in situ since 1850: 2. Biases and homogenization. Journal of Geophysical Research: Atmospheres, 116, D14104.

Kim, H.-S., G. A. Vecchi, T. R. Knutson, W. G. Anderson, T. L. Delworth, A. Rosati, F. Zeng, and M. Zhao, 2014: Tropical Cyclone Simulation and Response to CO2 Doubling in the GFDL CM2.5 High-Resolution Coupled Climate Model. Journal of Climate, 27, 8034-8054.

Klotzback, P. J., 2007: Recent developments in statistical prediction of seasonal Atlantic basin tropical cyclone activity. Tellus Series a-Dynamic Meteorology and Oceanography, 59, 511-518.

Knapp, K. R., M. C. Kruk, D. H. Levinson, H. J. Diamond, and C. J. Neumann, 2010: The International Best Track Archive for Climate Stewardship (IBTrACS). Bulletin of the American Meteorological Society, 91, 363-376.

Kobayashi, S., Y. Ota, Y. Harada, A. Ebita, M. Moriya, H. Onoda, K. Onogi, H. Kamahori, C. Kobayashi, H. Endo, K. Miyaoka, and K. Takahashi, 2015: The JRA-55 Reanalysis: General Specifications and Basic Characteristics. Journal of the Meteorological Society of Japan. Ser. II, 93, 5-48.

Kossin, J. P. and D. J. Vimont, 2007: A More General Framework for Understanding Atlantic Hurricane Variability and Trends. Bulletin of the American Meteorological Society, 88, 1767-1781.

Kucharski, F., I. S. Kang, R. Farneti, and L. Feudale, 2011: Tropical Pacific response to 20th century Atlantic warming. Geophysical Research Letters, 38.

Lee, H. S., T. Yamashita, and T. Mishima, 2012: Multi-decadal variations of ENSO, the Pacific Decadal Oscillation and tropical cyclones in the western North Pacific. Progress in Oceanography, 105, 67-80.

Li, X., S. Yang, H. Wang, X. Jia, and A. Kumar, 2013: A dynamical-statistical forecast model for the annual frequency of western Pacific tropical cyclones based on the NCEP Climate Forecast System version 2. Journal of Geophysical Research: Atmospheres, 118, 12,061-12,074.

Lin, I. I. and J. C. L. Chan, 2015: Recent decrease in typhoon destructive potential and global warming implications. Nat Commun, 6.

Liu, K. S. and J. C. L. Chan, 2012: Inactive Period of Western North Pacific Tropical Cyclone Activity in 1998–2011. Journal of Climate, 26, 2614-2630.

McGregor, S., A. Timmermann, M. F. Stuecker, M. H. England, M. Merrifield, F.-F. Jin, and Y. Chikamoto, 2014: Recent Walker circulation strengthening and Pacific cooling amplified by Atlantic warming. Nature Clim. Change, 4, 888-892.

Mitchell, C. L., 1932: West Indian Hurricanes and Other Tropical Cyclones of the North Atlantic Ocean. Monthly Weather Review, 60, 253-253.

Murakami, H., G. A. Vecchi, S. Underwood, T. Delworth, A. T. Wittenberg, W.Anderson, J. -H. Chen, R. Gudgel, L. Harris, S. -J. Lin, and F. Zeng, 2015:Simulation and prediction of Category 4 and 5 hurricanes in the high-resolution GFDL HiFLOR coupled climate model. J. Climate, in press

Nobre, P. and J. Shukla, 1996: Variations of Sea Surface Temperature, Wind Stress, and Rainfall over the Tropical Atlantic and South America. Journal of Climate, 9, 2464-2479.
Pielke Jr, R., J. Gratz, C. Landsea, D. Collins, M. Saunders, and R. Musulin, 2008: Normalized hurricane damage in the United States: 1900–2005. Natural Hazards Review, 9, 29.
Rappaport, E. N., 2000: Loss of Life in the United States Associated with Recent Atlantic Tropical Cyclones. Bulletin of the American Meteorological Society, 81, 2065-2073.
Schlesinger, M. E. and N. Ramankutty, 1994: An oscillation in the global climate system of period 65-70 years. Nature, 367, 723-726.
Servain, J., 1991: Simple climatic indices for the tropical Atlantic Ocean and some applications. Journal of Geophysical Research: Oceans, 96, 15137-15146.
Smirnov, D. and D. J. Vimont, 2010: Variability of the Atlantic Meridional Mode during the Atlantic Hurricane Season. Journal of Climate, 24, 1409-1424.
Trenberth, K. E. and D. J. Shea, 2006: Atlantic hurricanes and natural variability in 2005. Geophysical Research Letters, 33, 2006GL026894.
Tu, J. Y., C. Chou, and P. S. Chu, 2009: The Abrupt Shift of Typhoon Activity in the Vicinity of Taiwan and Its Association with Western North Pacific-East Asian Climate Change. Journal of Climate, 22, 3617-3628.
Vecchi, G. A. and B. J. Soden, 2007: Effect of remote sea surface temperature change on tropical cyclone potential intensity. Nature, 450, 1066-1070.
Vecchi, G. A., T. Delworth, R. Gudgel, S. Kapnick, A. Rosati, A. T. Wittenberg, F. Zeng, W. Anderson, V. Balaji, K. Dixon, L. Jia, H. S. Kim, L. Krishnamurthy, R. Msadek, W. F. Stern, S. D. Underwood, G. Villarini, X. Yang, and S. Zhang, 2014: On the Seasonal Forecasting of Regional Tropical Cyclone Activity. Journal of Climate, 27, 7994-8016.
Vimont, D. J. and J. P. Kossin, 2007: The Atlantic Meridional Mode and hurricane activity. Geophysical Research Letters, 34, L07709.
Vitart, F. D. and T. N. Stockdale, 2001: Seasonal forecasting of tropical storms using coupled GCM integrations. Monthly Weather Review, 129, 2521-2537.
Wang, B. and J. C. L. Chan, 2002: How strong ENSO events affect tropical storm activity over the Western North Pacific. Journal of Climate, 15, 1643-1658.
Wu, G. X. and N. C. Lau, 1992: A Gcm Simulation of the Relationship between Tropical-Storm Formation and Enso. Monthly Weather Review, 120, 958-977.
Wu, L., C. Wang, and B. Wang, 2015: Westward shift of western North Pacific tropical cyclogenesis. Geophysical Research Letters, 42, 1537-1542.
Xie, S.-P. and S. G. H. Philander, 1994: A coupled ocean-atmosphere model of relevance to the ITCZ in the eastern Pacific. Tellus A, 46, 340-350.
Yang, X., G. A. Vecchi, R. G. Gudgel, T. L. Delworth, S. Zhang, A. Rosati, L. Jia, W. F. Stern, A. T. Wittenberg, S. Kapnick, R. Msadek, S. D. Underwood, F. Zeng, W. Anderson, and V. Balaji, 2015: Seasonal Predictability of Extratropical Storm Tracks in GFDL's High-Resolution Climate Prediction Model. Journal of Climate, 28, 3592-3611.

Yu, J.-Y., P.-k. Kao, H. Paek, H.-H. Hsu, C.-w. Hung, M.-M. Lu, and S.-I. An, 2014: Linking Emergence of the Central Pacific El Niño to the Atlantic Multidecadal Oscillation. Journal of Climate, 28, 651-662.

Yu, J., T. Li, Z. Tan, and Z. Zhu, 2015: Effects of tropical North Atlantic SST on tropical cyclone genesis in the western North Pacific. Climate Dynamics, 1-13.

Zhan, R., Y. Wang, and X. Lei, 2010: Contributions of ENSO and East Indian Ocean SSTA to the Interannual Variability of Northwest Pacific Tropical Cyclone Frequency*. Journal of Climate, 24, 509-521.

Zhan, R., Y. Wang, and L. Tao, 2014: Intensified Impact of East Indian Ocean SST Anomaly on Tropical Cyclone Genesis Frequency over the Western North Pacific. Journal of Climate, 27, 8724-8739.

Zhang, H., A. Clement, and P. Di Nezio, 2013: The South Pacific Meridional Mode: A Mechanism for ENSO-like Variability. Journal of Climate, 27, 769-783.

Zhang, L. and C. Zhao, 2015: Processes and mechanisms for the model SST biases in the North Atlantic and North Pacific: A link with the Atlantic meridional overturning circulation. Journal of Advances in Modeling Earth Systems, 7, 739-758.

Zhang, R. and T. L. Delworth, 2007: Impact of the Atlantic Multidecadal Oscillation on North Pacific climate variability. Geophys. Res. Lett., 34, L23708.

Zhang, Q., Q. Liu, and L. Wu, 2009: Tropical Cyclone Damages in China 1983–2006. *Bulletin of the American Meteorological Society*, 90, 489-495.

Zhang, W., Y. Leung, and J. Min, 2013: North Pacific Gyre Oscillation and the occurrence of western North Pacific tropical cyclones. *Geophysical Research Letters*, 2013GL057691.

Zhang, W., Y. Leung, and K. Fraedrich, 2015a: Different El Niño Types and Intense Typhoons in the Western North Pacific. *Climate Dynamics*, 11-12, 2965-2977 .

Zhang, W., H. F. Graf, Y. Leung, and M. Herzog, 2012: Different El Niño Types and Tropical Cyclone Landfall in East Asia. *Journal of Climate*, 25, 6510-6523.

Zhang, W., G. Vecchi, H. Murakami, G. Villarini, L. Jia, 2015b: The Pacific Meridional Mode and the Occurrence of Tropical Cyclones in the Western North Pacific. *Journal of Climate*, in press.

Zhang, W., G.A. Vecchi, H. Murakami, T. Delworth, A.T. Wittenberg, W. Anderson, A. Rosati, S. Underwood, L. Harris, R. Gudgel, S.-J. Lin, G. Villarini, J-H Chen (2015c): Improved Simulation of Tropical Cyclone Responses to ENSO in the Western North Pacific in the High-Resolution GFDL HiFLOR Coupled Climate Model. *J. Climate*,under review after revision.

Table 1. TC frequency in the WNP and its sub-regions during peak season (JJASON) produced by the control experiment (CLIMO) and the perturbation experiment (PAMM). The boldface and "*" represent results that are significant at the 0.01 level.

TC Count	**WNP**	**SCS**	**NW**	**SW**	**SE**	**NE**
PAMM	19.9	2.4	3.2	11.4	2.4	0.5
CLIMO	23.6	2.8	4.1	9.9	5.5	1.3
Diff	**-3.7***	-0.4	**-0.9***	**1.5***	**-3.1***	**-0.8***

Figure captions:
Figure 1. The regression of SST (unit: °C) and 10m wind fields (ms^{-1}) onto the AMM index in observations during (a) 1970-2013 and (b) neutral ENSO years in this period. The blue (red) shading represents negative (positive) SST anomalies.
Figure 2 (a) The observed time series of WNP TC frequency (unit: times) and AMM index, and (b) the fitted lines of AMM and WNP TC frequency during 1970-2013 and neutral ENSO years in this period.
Figure 3. Regression of WNP TC track (a) and genesis (b) density (unit: times) onto the AMM index in observations. The TC track/genesis density is defined as those binned into every 5°×5° grid box without smoothing. The red lines divides the WNP into five sub-domains: SCS, NW, SW, NE, and SE in the long-term control experiment with FLOR.
Figure 4. Regression of GPI, 600 hPa relative humidity (unit: percent), 850 relative vorticity (unit: $10^{-6}s^{-1}$), zonal vertical wind shear (unit: m/s), and vertical profile (0 - 20°N) of zonal wind ($m \cdot s^{-1}$) and vertical velocity ($-100^*\omega$, $Pa \cdot s^{-1}$) onto the detrended AMM index. The shading represents minus omega ($-\omega$). The red lines divide the WNP into five subdomains: SCS, NW, SW, NE, and SE. Contours in bottom panel represent the climatology of zonal wind (unit: m/s).
Figure 5. Regression of SST (unit: °C) and 10m wind fields (ms^{-1}) onto the AMM index in the long-term control experiment with FLOR-FA.
Figure 6. The histogram of correlation coefficient between WNP TC frequency (unit: times) and the AMM index in every 45-year sub-periods. The red bar denotes the observed TC-AMM association.
Figure 7. The anomalous TC frequency in the WNP and its sub-domains (i.e., SCS, NW, SW, SE and NE as in Figures 3 and 4) during positive (blue) and negative (red) AMM years. The error bars represent the 0.95 confidence intervals. The symbol '*' following the names of the sub-regions (e.g., WNP and SCS) below x-axis indicates that the differences between negative and positive AMM years are significant at 0.05 level of significance.
Figure 8. Regression of TC track and genesis density (unit: times) onto the AMM index during strong AMM years when the magnitude of the AMM index is larger than one standard deviation. The red lines divides the WNP into five sub-domains: SCS, NW, SW, NE, and SE in the long-term control experiment with FLOR.
Figure 9. Regression of GPI, 600 hPa relative humidity (unit: percent), 850 relative vorticity (unit: $10^{-6}s^{-1}$), zonal vertical wind shear (unit: m/s), and vertical profile (0 - 20°N) of zonal wind ($m \cdot s^{-1}$) and vertical velocity ($-100^*\omega$, $Pa \cdot s^{-1}$) onto the AMM index in the WNP in the long-term control experiment with FLOR. The shading represents minus omega ($-\omega$). The red lines divides the WNP into five sub-domains: SCS, NW, SW, NE, and SE in the long-term control experiment with FLOR. Contours in bottom panel represent the climatology of zonal wind (unit: m/s).
Figure 10. The differences in WNP TC track and genesis density between PAMM and CLIMO experiments. The TC track/genesis density is obtained by binning TCs into every 5×5 grid box without smoothing. The red lines divides the WNP into five sub-domains: SCS, NW, SW, NE, and SE in the long-term control experiment with

FLOR.

Figure 11. Differences in GPI, 600 hPa relative humidity (unit: percent), 850 relative vorticity (unit: $10^{-6}s^{-1}$), zonal vertical wind shear (unit: m/s), and vertical profile (0 - 20°N) of zonal wind ($m \cdot s^{-1}$) and vertical velocity ($-100*\omega$, $Pa \cdot s^{-1}$) between the PAMM and CLIMO experiments with FLOR-FA. The contours in bottom panel (e) represent the climatology of zonal wind (unit: m/s) in the CLIMO experiment. The shading represents minus omega ($-\omega$). The red lines divides the WNP into five sub-domains: SCS, NW, SW, NE, and SE in the long-term control experiment with FLOR.

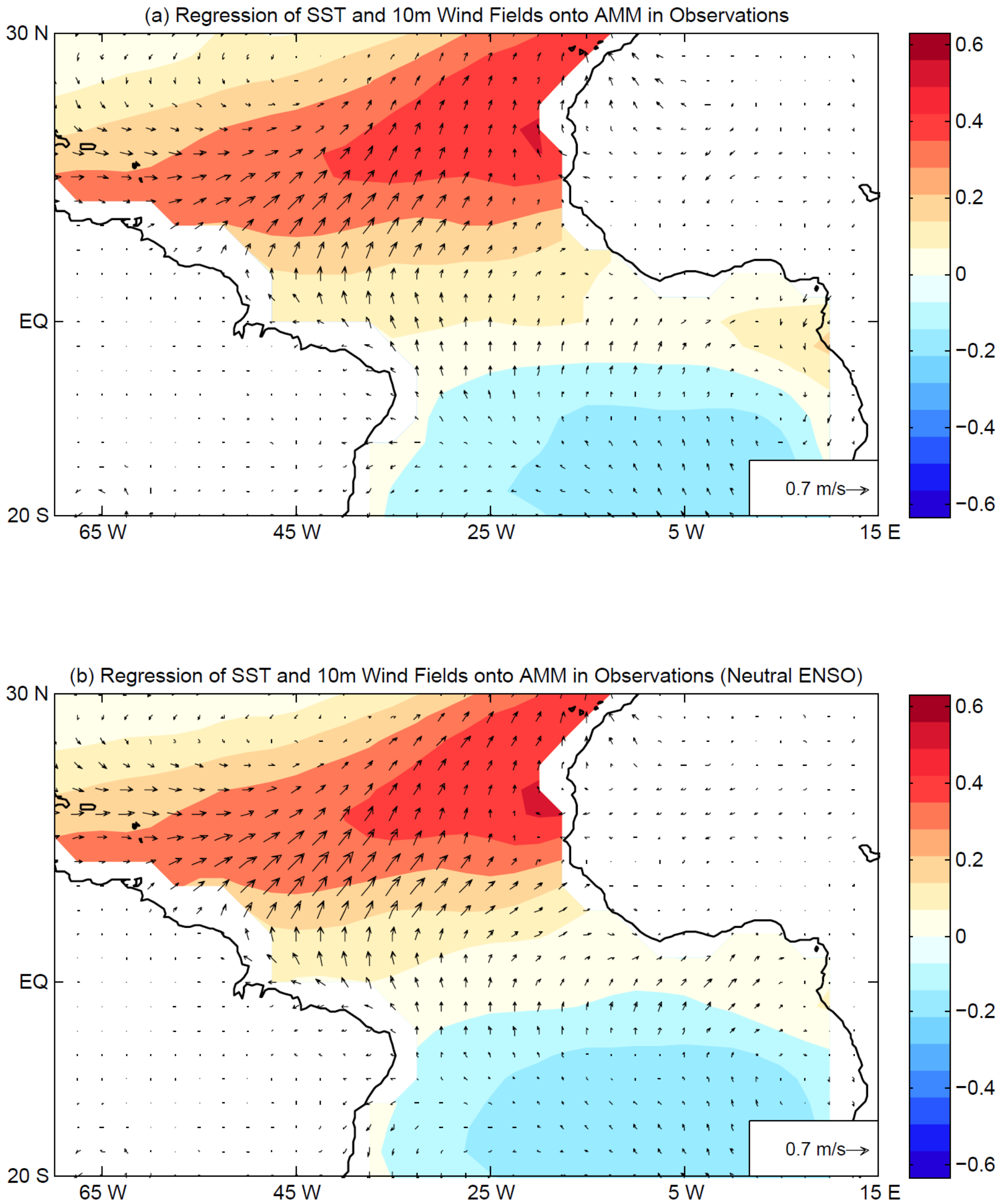

Figure 1. The regression of SST (unit: °C) and 10m wind fields (ms^{-1}) onto the AMM index in observations during (a) 1970-2013 and (b) neutral ENSO years in this period. The blue (red) shading represents negative (positive) SST anomalies.

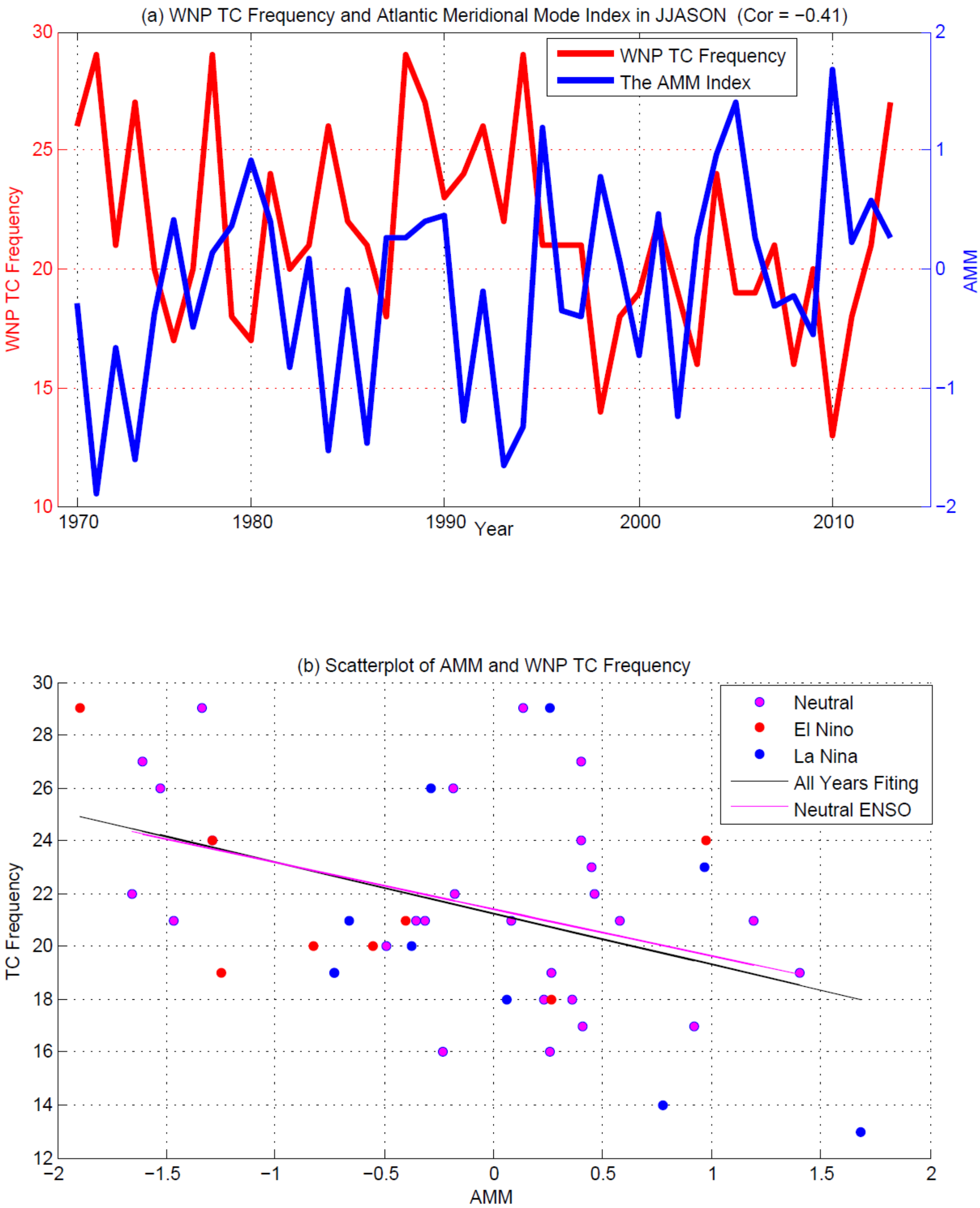

Figure 2 (a) The observed time series of WNP TC frequency (unit: times) and AMM index, and (b) the fitted lines of AMM and WNP TC frequency during 1970-2013 and neutral ENSO years in this period.

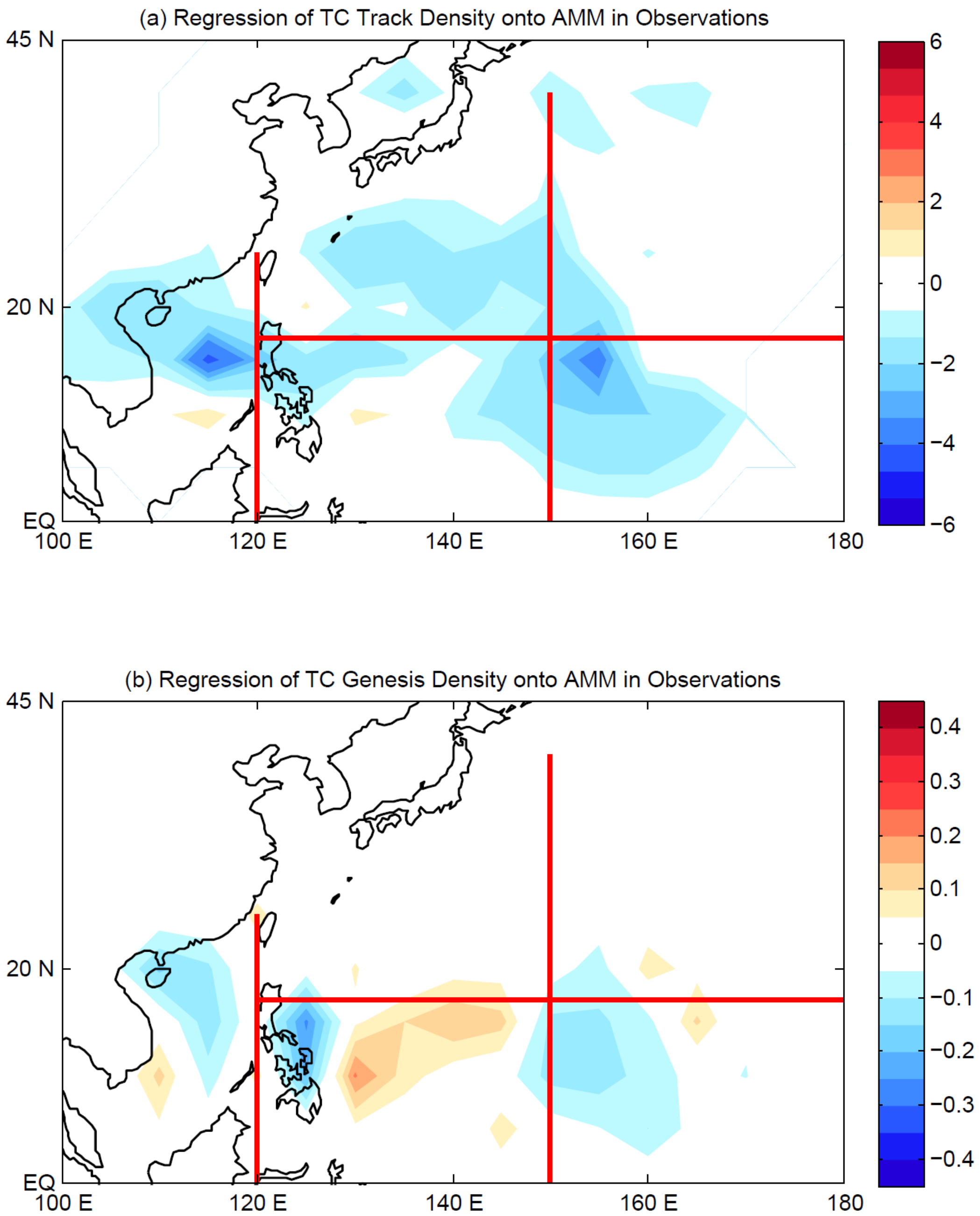

Figure 3. Regression of WNP TC track (a) and genesis (b) density (unit: times) onto the AMM index in observations. The TC track/genesis density is defined as those binned into every 5°×5° grid box without smoothing. The red lines divides the WNP into five sub-domains: SCS, NW, SW, NE, and SE in the long-term control experiment with FLOR.

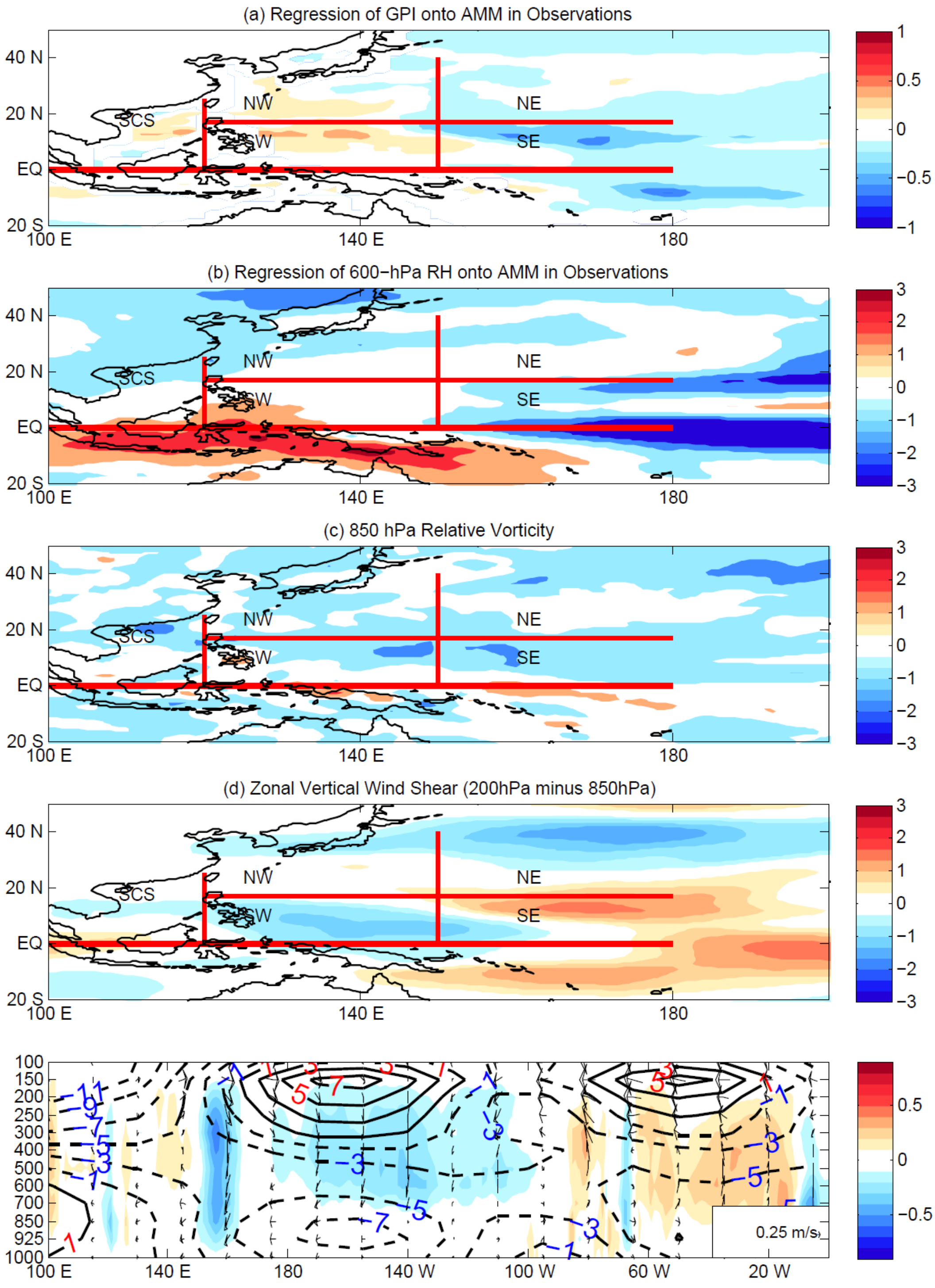

Figure 4. Regression of GPI, 600 hPa relative humidity (unit: percent), 850 relative vorticity (unit: $10^{-6}s^{-1}$), zonal vertical wind shear (unit: m/s), and vertical profile (0 - 20°N) of zonal wind ($m{\cdot}s^{-1}$) and vertical velocity ($-100{*}\omega$, $Pa{\cdot}s^{-1}$) onto the detrended AMM index. The shading represents minus omega ($-\omega$). The red lines divide the WNP into five subdomains: SCS, NW, SW, NE, and SE. Contours in bottom panel represent the climatology of zonal wind (unit: m/s).

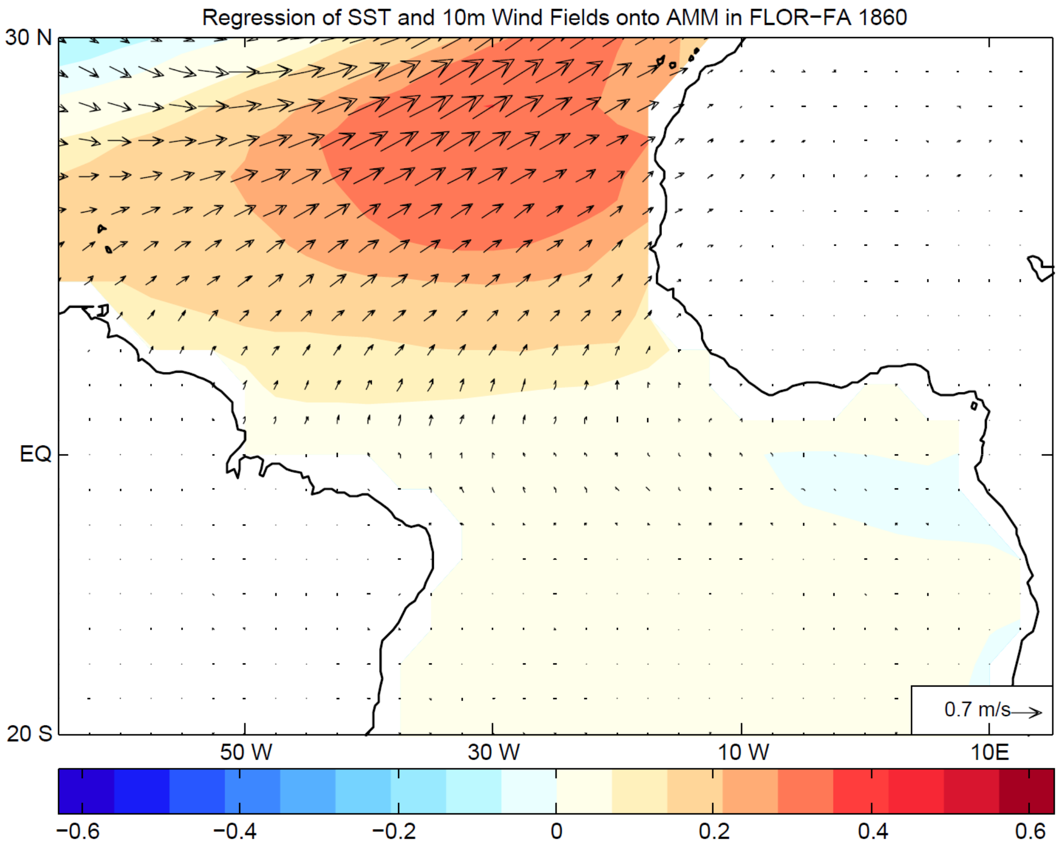

Figure 5. Regression of SST (unit: °C) and 10m wind fields (ms^{-1}) onto the AMM index in the long-term control experiment with FLOR-FA.

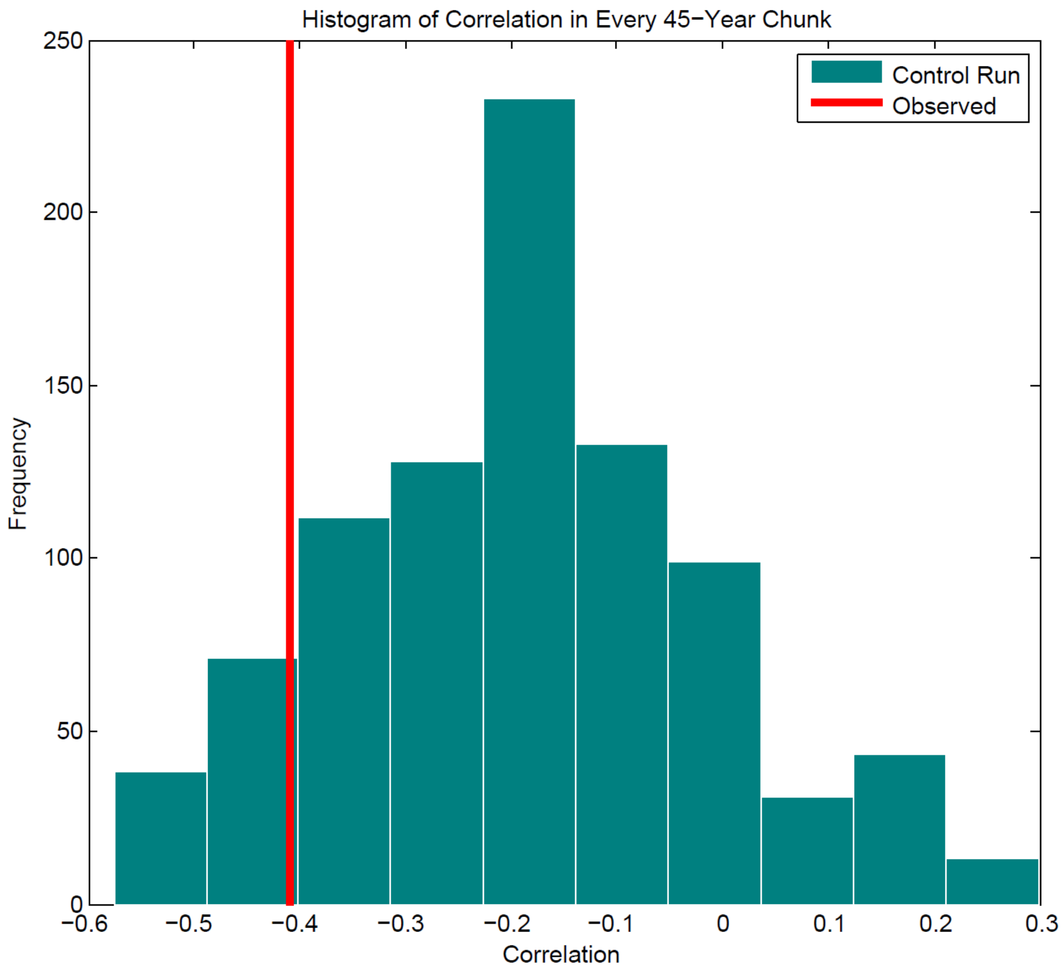

Figure 6. The histogram of correlation coefficient between WNP TC frequency (unit: times) and the AMM index in every 45-year sub-periods. The red bar denotes the observed TC-AMM association.

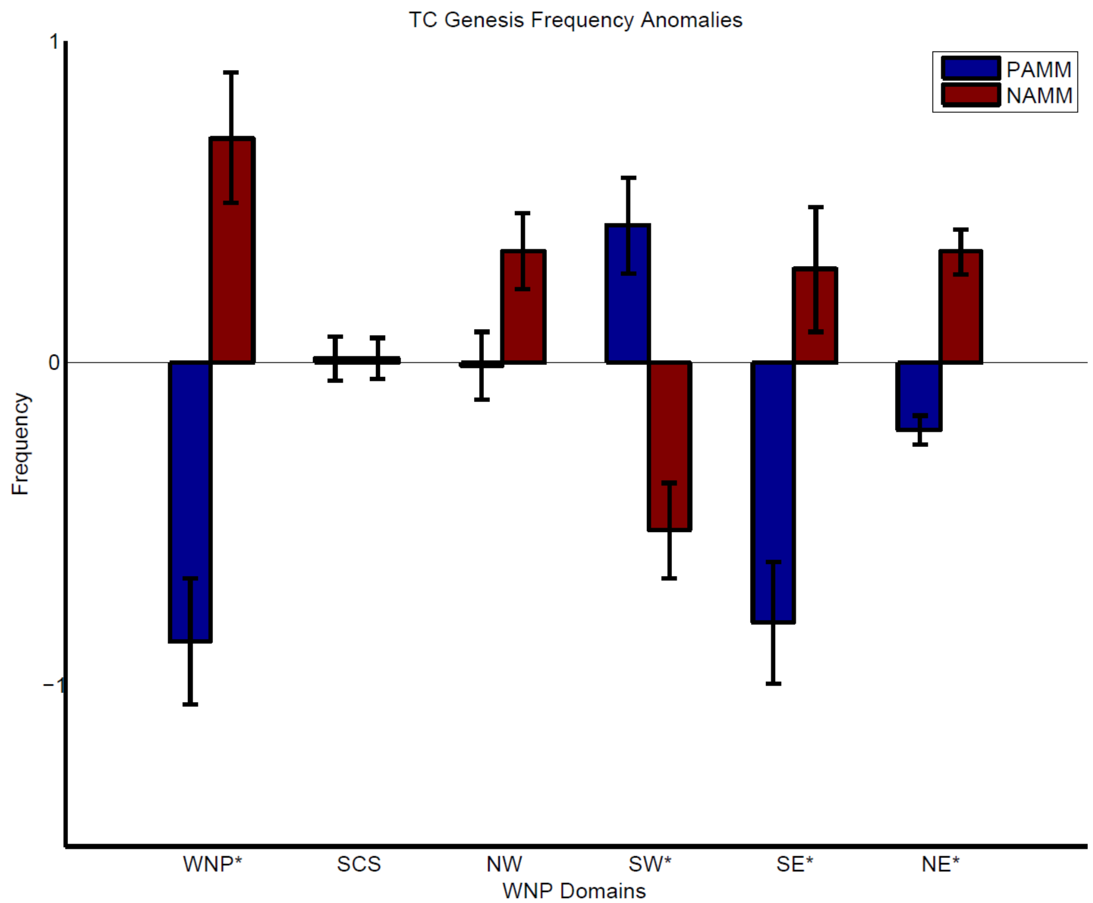

Figure 7. The anomalous TC frequency in the WNP and its sub-domains (i.e., SCS, NW, SW, SE and NE as in Figures 3 and 4) during positive (blue) and negative (red) AMM years. The error bars represent the 0.95 confidence intervals. The symbol '*' following the names of the sub-regions (e.g., WNP and SCS) below x-axis indicates that the differences between negative and positive AMM years are significant at 0.05 level of significance.

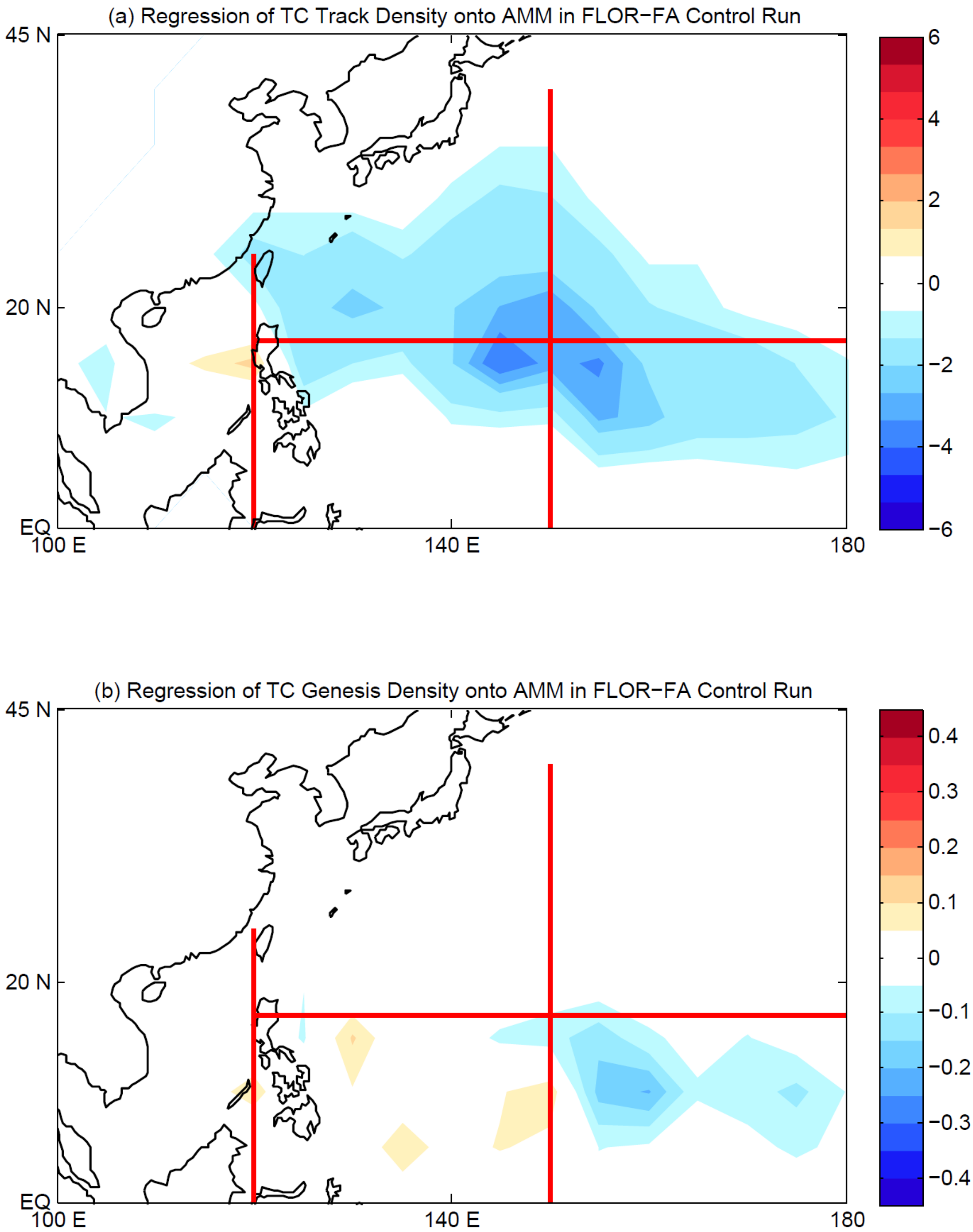

Figure 8. Regression of TC track and genesis density (unit: times) onto the AMM index during strong AMM years when the magnitude of the AMM index is larger than one standard deviation. The red lines divides the WNP into five sub-domains: SCS, NW, SW, NE, and SE in the long-term control experiment with FLOR.

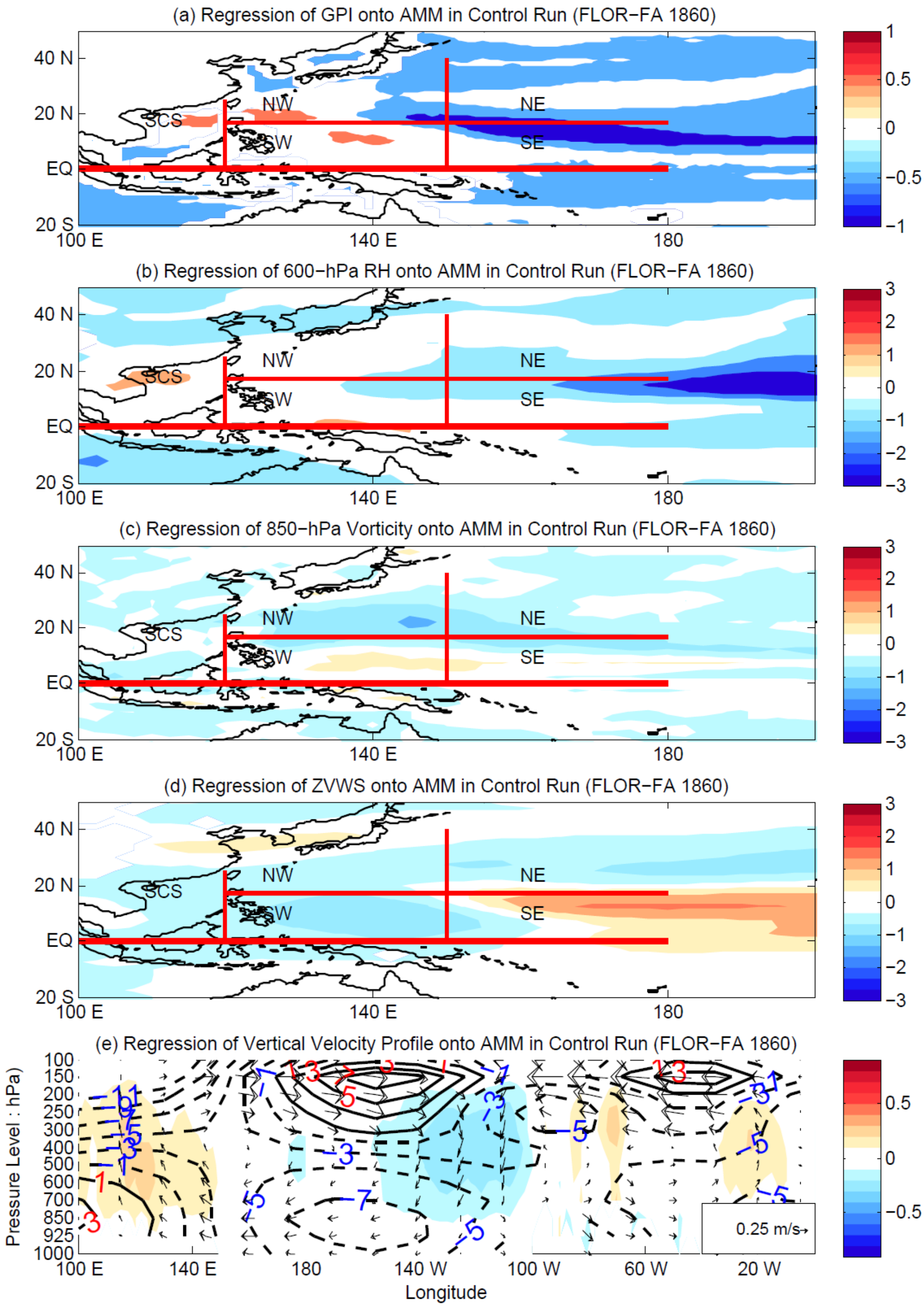

Figure 9. Regression of GPI, 600 hPa relative humidity (unit: percent), 850 relative vorticity (unit: $10^{-6}s^{-1}$), zonal vertical wind shear (unit: m/s), and vertical profile (0 - 20°N) of zonal wind ($m{\cdot}s^{-1}$) and vertical velocity ($-100{*}\omega$, $Pa{\cdot}s^{-1}$) onto the AMM index in the WNP in the long-term control experiment with FLOR. The shading

represents minus omega (-ω). The red lines divides the WNP into five sub-domains: SCS, NW, SW, NE, and SE in the long-term control experiment with FLOR. Contours in bottom panel represent the climatology of zonal wind (unit: m/s).

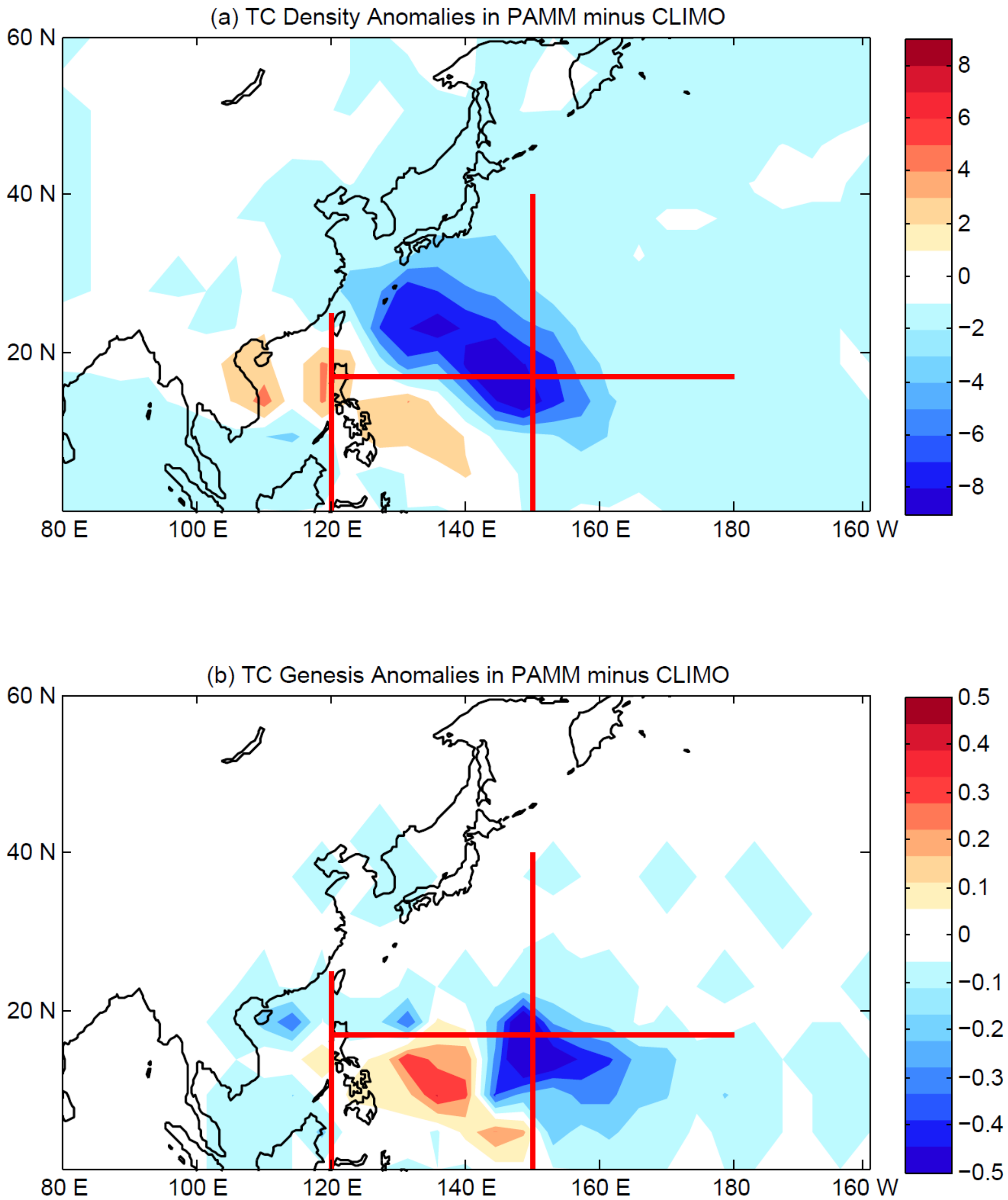

Figure 10. The differences in WNP TC track and genesis density between PAMM and CLIMO experiments. The TC track/genesis density is obtained by binning TCs into every 5×5 grid box without smoothing. The red lines divides the WNP into five sub-domains: SCS, NW, SW, NE, and SE in the long-term control experiment with FLOR.

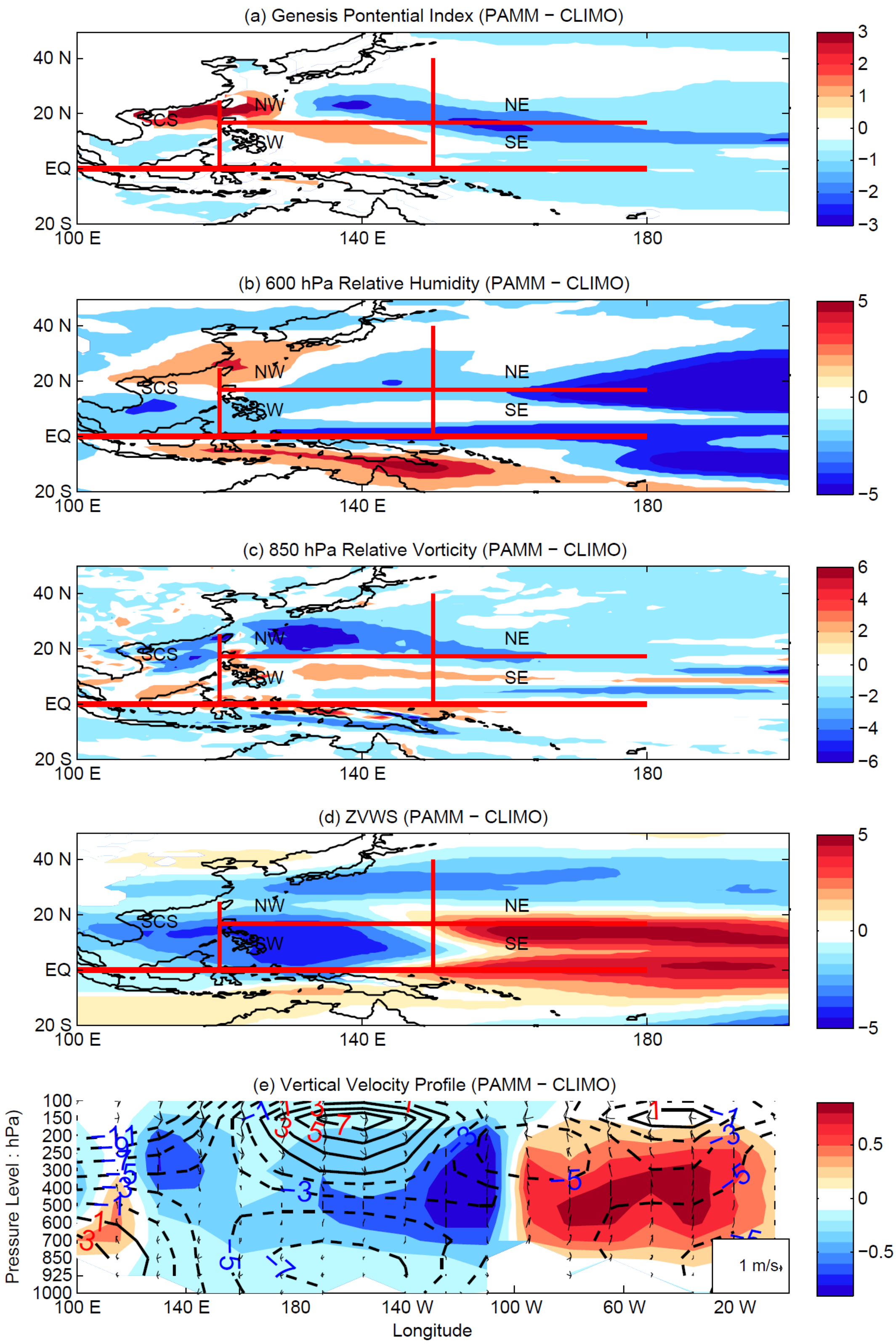

Figure 11. Differences in GPI, 600 hPa relative humidity (unit: percent), 850 relative vorticity (unit: $10^{-6}s^{-1}$), zonal vertical wind shear (unit: m/s), and vertical profile (0 - 20°N) of zonal wind ($m{\cdot}s^{-1}$) and vertical velocity ($-100^{*}\omega$, $Pa{\cdot}s^{-1}$) between the PAMM and CLIMO experiments with FLOR-FA. The contours in bottom panel (e) represent the climatology of zonal wind (unit: m/s) in the CLIMO experiment. The

shading represents minus omega (-ω). The red lines divides the WNP into five sub-domains: SCS, NW, SW, NE, and SE in the long-term control experiment with FLOR.